Acta Oceanol. Sin., 2020, Vol. 39, No. 12, P. 121–134
https://doi.org/10.1007/s13131-020-1684-z
http://www.hyxb.org.cn
E-mail: hyxbe@263.net

Sand barrier morphological evolution based on time series remote sensing images: a case study of Anhaiao, Pingtan

Heshan Lin[1, 2], Xingguang Yu[3], Zhigang Yu[1], Yikang Gao[2], Jinyan Xu[2]*, Aiping Feng[2], Zhijun Liu[4], Degang Jiang[2], Fan Yu[2]

[1] College of Environmental Science and Engineering, Ocean University of China, Qingdao 266100, China

[2] Island Research Center, Ministry of Natural Resources, Pingtan 350400, China

[3] Third Institute of Oceanography, Ministry of Natural Resources, Xiamen 361005, China

[4] Ministry of Natural Resources, Beijing 100812, China

Received 28 October 2019; accepted 28 July 2020

Abstract

The morphological evolution of the sand barrier in the Anhaiao coastal zone of Pingtan from 1996 to 2018 was studied. Tidal correction was used to refine the location of the coastline. A standard deviation ellipse method was applied to further analyze the movement of the barrier head with the axis and rotation angle. A natural neighbor interpolation (NNI) method was carried out to calculate the terrain of the intertidal area, and the erosion and deposition characteristics were illustrated based on the terrain. The results showed that the northern part of the sand barrier facing the lagoon area was deposited over the whole studied period, while erosion has always occurred in the southern part of the sand barrier facing the open sea. The erosion and deposition were slightly different on both sides of the barrier head due to hydrodynamic turbulence. The middle sand barrier moved 102.60 m away from its original location in 1996, and the end of the barrier moved 65.45 m. The head of the sand barrier continued moving 379 m to the northwest. Consequently, the preliminary morphological evolution of the sand barrier corresponding to the distance and direction of movement was detected.

Key words: sand barrier, dynamic evolution, movement, reclamation

Citation: Lin Heshan, Yu Xingguang, Yu Zhigang, Gao Yikang, Xu Jinyan, Feng Aiping, Liu Zhijun, Jiang Degang, Yu Fan. 2020. Sand barrier morphological evolution based on time series remote sensing images: a case study of Anhaiao, Pingtan. Acta Oceanologica Sinica, 39(12): 121–134, doi: 10.1007/s13131-020-1684-z

1 Introduction

With the development of the Chinese economy and high population growth, most people have been moving to the developed cities in coastal areas (Lin et al., 2016), and the demand for marine resources has become increasingly severe, which has caused unrecoverable changes to certain marine ecosystems of impacted sea areas and islands. As a unique coastal ecosystem, the sand barrier-lagoon landscape performs important ecological functions, plays an important role for local residents (Tiner et al., 2015; Wang, 2009; Sun, 2013; Chen, 2011) and has suffered great pressures from natural factors and human activities. It is necessary to monitor the changes of sand barrier-lagoons to better understand the geomorphological evolution of the barriers.

From the geomorphological evolution process, the internal relationship between coastline change, sediment transport and sea-level rise had been studied, and the multi-stage evolution model of sand barrier and lagoon was proposed (Ghezzo et al., 2010; Carrasco et al., 2016; Duck and da Silva, 2012; Storms et al., 2008; FitzGerald et al., 2006). The research results show that due to many factors such as sea level rise, nearshore hydrodynamic environment, continental shelf formation patterns, sediment sources and transportation processes, the geomorphological evolution models of sand barrier lagoon present the diversified characteristics. However, one of the factors mentioned above may play a leading or even decisive role at some stages of sand barrier evolution.

Recently, an increasing number of researchers have focused on the geomorphological evolution of sand barriers with the development of time series remote sensing images (Frihy et al., 1998; El-Asmar and Hereher, 2011; Kent and Mast, 2005; El-Asmar et al., 2013; Ahmed et al., 2009; Alonso-Pérez et al., 2003; Dronova et al., 2011; Chang et al., 2018; Brivio and Zilioli, 1996; Han et al., 2015; Sun et al., 2016; Gu et al., 2005).

Landsat satellite image data and a series of topographic maps covering a 86-years monitoring period were used to analyze the shoreline erosion and accretion, evolution of Damietta coastal spit and changes in the lagoon margin and contiguous islands across the Damietta promontory of the Nile Delta in Egypt (Frihy et al., 1998). A set of four satellite images from the multi-spectral scanner, thematic mapper and Systeme Pour l'Observation de la Terre sensors were utilized in order to estimate the spatio-temporal coastal changes that occurred in the Manzala Lagoon area in Egypt between 1973 and 2007 (El-Asmar and Hereher, 2011). A set of six satellite images acquired between 1973 and 2011 were employed to map the change of the surface area of the Burullus Lagoon in the Nile Delta using the water indices approach (El-Asmar et al., 2013). Through the analysis of a series of satellite-derived images between 1974 and 2015 in the Cigu Lagoon in

Foundation item: The Key Projects of Philosophy and Social Sciences Research, Ministry of Education under contract No. 18JZD059.
*Corresponding author, E-mail: xujy_liesmars@whu.edu.cn

southwestern Taiwan, the results revealed that human activities, including the construction of hard structures along the coastline and along an upstream reservoir, altered the balance of sediment transmission and resulted in the retreat and erosion of barrier sandbars along the coast, and the lagoon evolution model revealed that the Cigu Lagoon may disappear in the future (Chang et al., 2018). The changes in different isobaths and calculation of scouring and silting in different sea maps in Bohe sand barrier-lagoon in Southeast China were analyzed by Dai et al. (2007). The results suggested that dynamic accreted equilibrium state existed near the area of waterline in the coast, where the changes of scouring and silting of the nearshore zone was weak and the seafloor in this study area had a relatively stable state. Through the multi-stage remote sensing images analysis combined with field measurements, these studies have carried out researches on the extraction technology of shoreline position, and analyzed the evolution process of sand bar and lagoon, including the morphodynamic process and features of coastal sandy bar under the combined effects of normal waves, tidal currents, river runoff, floods and storm surge.

The Anhaiao barrier-lagoon geomorphological system is one of the most important tourism resources for the Pingtan international tourism island in Fujian Province, China. In recent years, the sand barrier has been deposited inside the lagoon, and the outside of the barrier has been retreated, a process was affected by human reclamation activities, and the barrier landscape has become more vulnerable (Lin et al., 2016). Therefore, the study of the barrier geomorphological evolution of the barrier-lagoon system is necessary to figure out the principle of changes and the driven factors. Figure 1 shows the location of the study area.

In this study, a series of barrier coastlines was extracted using 12 multi-temporal remote sensing images and ground survey data with tidal corrections from 1996 to 2018. Analysis of the barrier terrain based on GIS interpolation was carried out simultaneously. Furthermore, the detailed geomorphological evolution of the barrier was analyzed. Finally analysis of the driven factors was also carried out with the countermeasures for the protection of the barrier approved.

2 Methodology

2.1 *Coastline extraction and tidal corrections*

2.1.1 *Coastline extraction*

The modified normalized difference water index (MNDWI) (Eq.(1)), proposed by Xu (2005), and manual extraction were used to extract the instantaneous water-land boundary as the coastline.

$$\mathrm{MNDWI} = \frac{\mathrm{Green} - \mathrm{MIR}}{\mathrm{Green} + \mathrm{MIR}}, \tag{1}$$

where Green and MIR represent the reflectance of the green and middle infrared bands. MNDWI is the world's most widely used water body index, which was generally used as the most important technique for identifying wetlands and distinguishing between water and non-aqueous information (Zheng and Bastiaanssen, 2013; Chen and Mueller, 2018; Allen and Pavelsky, 2018; Murray et al., 2019). The maximum error for instantaneous water-land boundary extraction using MNDWI is limited in 1 pixel. In this study, MNDWI was used to extract instantaneous coastline by Landsat and Worldview2 images. Manual extraction was performed to the other images according to the image character-

Fig. 1. Anhaiao barrier-lagoon system.

istics of feature on the image, such as hue, shape, size and texture, etc. Coastlines extracted here were not used directly to analyze the changes among difference time series. They were just applied as the initial lines which tidal corrections would be carried out in the following.

2.1.2 *Tidal corrections*

(1) Principle of the tidal corrections

Because of the different tides of the 13 satellite images, the coastlines extracted above could not be used directly to show the changes of the barrier. The average high tide and average low tide from 1996 to 2006 were used as the target tides for the corrections. Based on the extracted coastlines, the instantaneous low-tide coastline was corrected to the target low-tide coastline, while the instantaneous high-tide coastline was corrected to the target high level (Fig. 2). Finally, the real coastline was determined.

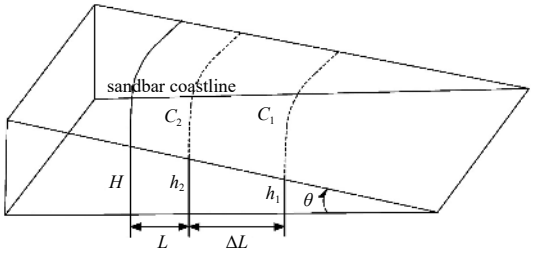

Fig. 2. The principle of tidal corrections.

The instantaneous coastlines C_1 and C_2 of different images were extracted, and the ground distance ΔL between each C_1 and C_2 pair was measured (Fig. 2).

Assume that the slope of the terrain is constant, and the aspect is the normal direction of C_1 and C_2, where h_1 and h_2 represent the elevation of C_1 and C_2. The slope can be expressed as

$$k = \frac{h_2 - h_1}{\Delta L} = \tan\theta. \tag{2}$$

With the target elevation H and the tide h of the image, the horizontal bias can be calculated as

$$L = \frac{H - h}{k}. \tag{3}$$

The refined coastline of each image can be corrected as above.

(2) Tidal corrections

The tidal correction mentioned previously is usually suitable for large-scale areas, with the hypothesis that the slope of the whole coastal area is constant. However, this hypothesis is not the situation of barrier terrain. A segmentation strategy was applied for the coastline tidal correction of the whole barrier (Fig. 3): The segmentation was first carried out to the extracted high-tide coastline of the barrier every 30 m, and the central point of each sample was selected as the split point. The extracted low-tide coastline was segmented according to the distributed split points selected previously.

The distance between the high-tide and the low-tide coastline was calculated as follows. The slope of each sample and the tide difference were calculated according to the tidal correction principle.

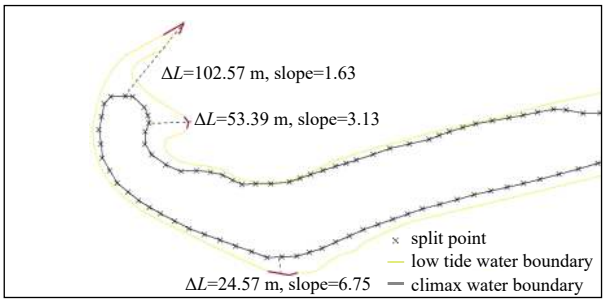

Fig. 3. Diagram of the segmentation strategy.

2.2 *Sand barrier morphological evolution*

2.2.1 *Evolution of the barrier head*

Based on the refined coastlines, the geomorphological changes of the barrier were detected first. However, the shape of the barrier head is more complicated by wave and hydrodynamic factors. Hence, the standard deviation ellipse algorithm, developed by Lefever (1926), was applied to analyze the evolution of the barrier head (Fig. 4). The long axis, the short axis and the rotation angle of the ellipse determined the distribution and the direction of certain data:

$$\mathrm{SDE}_x = \sqrt{\frac{\sum_{i=1}^{n}(x_i - \tilde{x}_i)^2}{n}}, \tag{4}$$

$$\mathrm{SDE}_y = \sqrt{\frac{\sum_{i=1}^{n}(y_i - \tilde{y}_i)^2}{n}}, \tag{5}$$

where x_i and y_i represent the coordinates of feature i, $(\tilde{x}_i, \tilde{y}_i)$ represents the two axes of the ellipse, and n represents the number of features. The rotation angle can be expressed as

$$\tan\theta = \frac{\left(\sum_{i=1}^{n}\tilde{x}_i^2 - \sum_{i=1}^{n}\tilde{y}_i^2\right) + \sqrt{\left(\sum_{i=1}^{n}\tilde{x}_i^2 - \sum_{i=1}^{n}\tilde{y}_i^2\right)^2 + 4\left(\sum_{i=1}^{n}\tilde{x}_i\tilde{y}_i\right)^2}}{2\sum_{i=1}^{n}\tilde{x}_i\tilde{y}_i}, \tag{6}$$

where $\tilde{x}_i$ represents the difference between the average x of all features and the x_i.

The standard deviation of the X and Y axes can be detailed as follows:

$$\sigma_x = \sqrt{2}\sqrt{\frac{\sum_{i=1}^{n}(\tilde{x}_i\cos\theta - \tilde{y}_i\cos\theta)^2}{n}}, \tag{7}$$

$$\sigma_y = \sqrt{2}\sqrt{\frac{\sum_{i=1}^{n}(\tilde{x}_i\sin\theta + \tilde{y}_i\sin\theta)^2}{n}}. \tag{8}$$

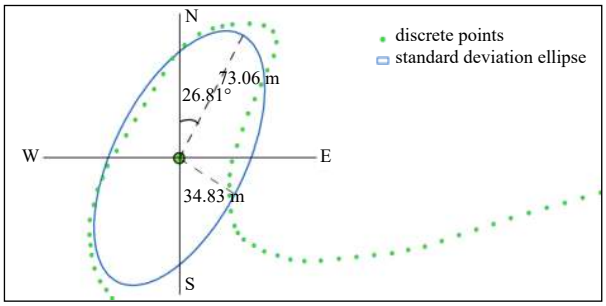

Fig. 4. Diagram of the standard deviation ellipse. Half of the long axis length is 73.06 m, half of the short axis length is 34.83 m, and the rotation angle of the standard deviation ellipse is 26.81°.

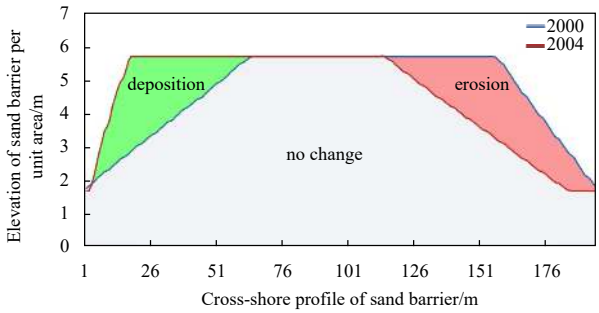

Fig. 5. Diagram of elevation calculation of sand barrier per unit area.

When a feature has a spatially normal distribution, a standard deviation range will include a centroid with approximately 68% of all point features, two standard deviations will include approximately 95% of all point features, and three standard deviations will cover approximately 99% of the point features. The rotation angle of the standard deviation ellipse determines the direction of the barrier head. The evolution of the sand barrier can be reflected as the changes in the coastline and the rotation angles of different images.

2.2.2 *Deposition and erosion of the barrier*

Natural neighbor interpolation was used to calculate the barrier terrain based on the average low tide H_t1 and average high tide H_t2 correction (Sibson, 1981). This method is a local interpolation focused on the samples around the target to ensure the interpreted elevation is located in the tidal range of the area. The interpolated elevation of the target point can be described as follows:

$$G(x,\ y) = \sum_{i=1}^{n} w_i f(x_i,\ y_i), \tag{9}$$

where w_i represents the weight that contributed to $G(x, y)$, and $f(x_i,\ y_i)$ represents the elevation of point $(x_i,\ y_i)$.

Based on the interpolation terrain of the barrier, the volume ($\mathrm{Vol_r}$) of the deposition and erosion can be calculated as

$$\mathrm{Vol_r} = (\mathrm{Ele_2} - \mathrm{Ele_1})\,\mathrm{PixSize}, \tag{10}$$

where $\mathrm{Pixsize}$ represents the spatial resolution of the terrain, $\mathrm{Ele_1}$ and $\mathrm{Ele_2}$ represent the elevations of sand barrier per unit area at early time and late time, respectively. As the interpolated elevation was between H_t1 and H_t2, the elevations lower than H_t1 were interpolated with the tide difference and the slope of the barrier. Figure 5 shows a diagram of the calculations of elevation of sand barrier per unit area.

2.3 *Study area and datasets*

The Anhaiao Bay is located on the east coast of the Haitan Strait and southwest of Haitan Island (Fig. 6). The bay is a widely developed lagoon coastal area with the famous Jianmin sand barrier. An area with unique scenery, the barrier extends approximately 3 km into the sea and is affected by the interaction of siltation and erosion. During the last 20–30 years, beginning in 1996, the barrier has changed substantially because of high amounts of human exploitation and the development of the surrounding open sea, such as reclamation projects for harbor construction and mariculture.

Further analysis shows that a regular half-day tide is the dominant tide in this area. There are two high tides and two low tides, and the difference between these tides is relatively small. The tides increase from the mouth to the middle of the area during high tides and decrease in the same direction during low tides. Figure 7 shows the relationship of the elevation datum of the coastal zones in Pingtan. Figure 8 and Table 1 show the locations and characteristics of the temporary tidal observation sites.

Given the availability of the satellite images and the spatial resolution for the study, the images obtained in the 1980s were hardly suitable for the extraction of the barrier changes. Twelve multi-temporal remote sensing images since the 1990s, charts and hydrodynamic data of different periods, and topographic survey data of the Anhaiao Bay in Pingtan, including the sand barrier, were collected. The spatial resolution of the images was approximately 0.46–15 m. The tidal difference between the two images in each year was approximately 3 m to ensure accuracy. Table 2 shows the details of the 12 images.

In order to extract the coastline of different period and decrease the scale factors, all the images were geometric and radiometric calibrated and georegistered to the aerial orthophoto acquired in 2008. The accuracy for georegistration was 0.5 pixel, with the maximum error 7.5 m according to the spatial resolution. The coastline of each image was extracted respectively and transferred into vector data. Changes of different coastlines were compared across different vector data instead of the raster data.

3 Results and discussion

3.1 *The morphological changes of the main barrier*

Based on the tide data in Table 1, the average low tide H_t1 and average high tide H_t2 were estimated to be 171 cm and 570 cm, respectively. The 12 images were processed according to the workflow described in the previous section, and the corresponding refined coastline was extracted (Fig. 9).

Six of the images were selected for the geomorphological change analysis of the barrier. The coastlines of 2015 and 2018 were obtained from ground survey data with RTK. Two profiles are set as A and B in Fig. 10 to depict the location movements of the barrier.

Table 3 depicts the movement of the barrier. The results show that most of the movements occurred in the periods of 1996–2000, 2004–2006 and 2006–2018, and the barrier moved northward. The middle part of the barrier moved 102.60 m away from its original location, and the end of the barrier moved 65.45 m.

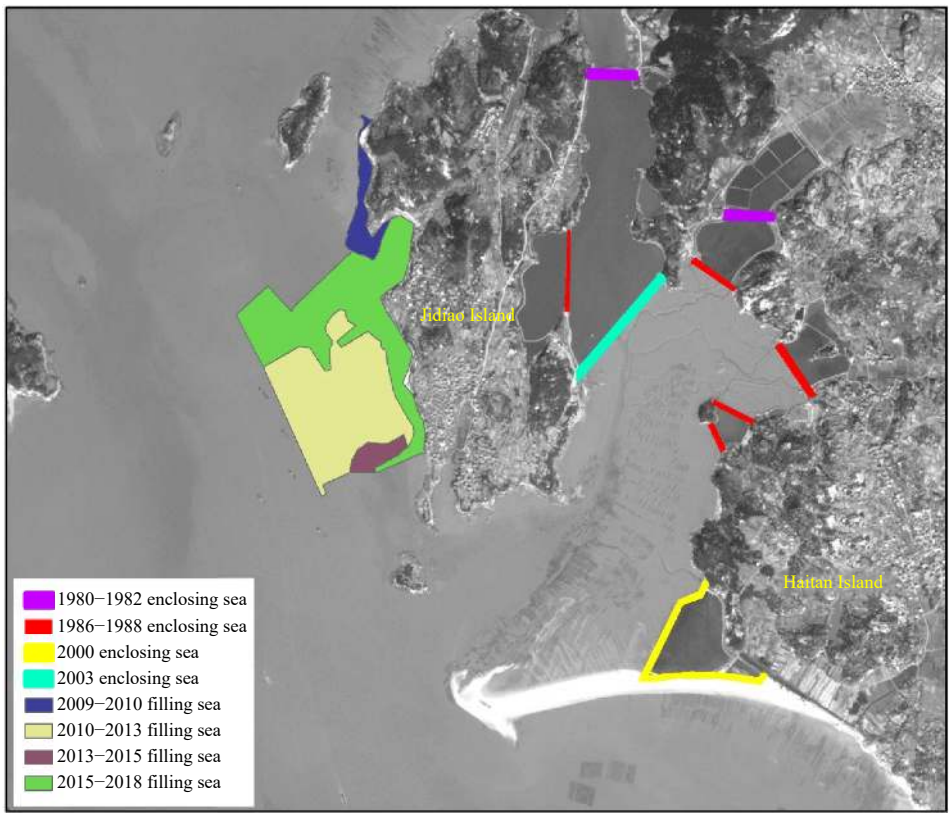

Fig. 6. Exploitations of the Anhaiao barrier-lagoon area.

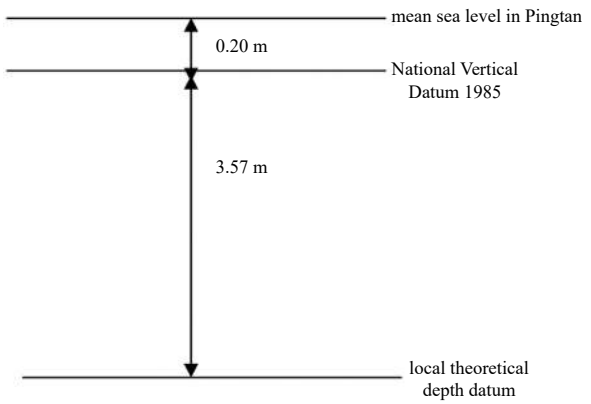

Fig. 7. Relationship of each elevation datum of coastal zones in Pingtan.

The movement rate of the sand barrier reached a peak of 9.59 m/a in 2004 and decreased to 0.45 m/a in 2013.

Further analysis revealed that the end of the barrier moved 26.88 m northward at a high rate of approximately 6.72 m/a, while the middle part of the barrier moved 32.28 m at a rate of 9.57 m/a from June 1996 to December 2000; the main reason for these movements was reclamation for mariculture. During the period of December 2000 to November 2004, the barrier end continued moving 10.54 m northward at an average rate of approximately 2.63 m/a. However, the movement rate of the middle barrier reached a peak of approximately 9.59 m/a, moving a distance of 76.64 m from the position in 1996. From November 2004 to December 2006, the whole barrier continued moving northward at a high rate, with the end and middle of the barrier moving 45.97 m and 94.74 m, respectively. The movement rate slowed between 2006 and 2010 as the human activities around the barrier and the surrounding sea decreased. The movement rate decreased to minimum of 1.35 m/a at the end of the barrier and 0.45 m/a in the middle of the barrier from 2010 to 2013. Deposition occurred in the northern part of the barrier facing the lagoon as mariculture increased in the lagoon area, while erosion occurred in the part of the barrier facing the open sea. The coastlines acquired from the ground survey data in 2015 and 2018 showed that the sand barrier was still moving to the north at a low average rate of 1.10 m/a at the end part and 0.47 m/a in the middle part of the barrier.

3.2 *Morphological changes of the barrier head*

Figure 11 shows the characteristics of the barrier head changes. Similar to the dynamic changes of the middle and end parts of the barrier, the barrier head also kept moving to the north from 1996 to 2018. During the period of 1996 to 2004, the shape of the barrier head changed obviously, and the center of the ellipses kept moving to the north with a clockwise rotation. In 1996, there were two inflection points extending to the sea in the northeast and southeast, and the main extension direction was the northeast. In 2004, a new inflection point extending to the sea in the northwest was developed, and the distance between the ellipse center and the southeast inflection point was 241 m, with a distance of 338 m to the northeast. The rotation angle was northeast 57.04° with a clockwise rotation increase of 30.2°.

In the following period from 2004 to 2010, the standard deviation ellipse center of the barrier head continued moving to the west and northwest, and three inflection points developed as

Fig. 8. Locations of tidal elevation observation sites.

Table 1. Tidal eigenvalue at each temporary tidal observation station

Factor	T1 Qianbianao station
Average tide/cm	21
High tide/cm	345
Low tide/cm	–335
Average high tide/cm	249
Average low tide/cm	–211
Average tide difference/cm	461
Maximum tide difference/cm	668
Minimum tide difference/cm	243
Average flood tide duration	6 h 1 min
Average ebb tide duration	6 h 23 min
Data time	April 1–30, 2016
Tidal datum	National Vertical Datum 1985

northeast, northwest and southeast when the head extended to the open sea. The northwest direction became the predominant direction from 2004 to 2006, and the northeast extension shortened from 338 m to 236 m. The rotation angle was northwest 52.97° until 2010; in comparison, this angle was northeast 57.04° in 2004. The distance between the center and the southeast point shortened to 222 m in 2010, while that between the center and the northwest increased to 215 m.

The shape of the barrier remained relatively stable from 2010 to 2018. The barrier head extended to the northwest with the disappearance of the northeast extension. The ellipse center was 333 m away from the southeast extension and 176 m from the axis extension northwest. The rotation angle was 6.8° with a clockwise rotation of 46.18° from the orientation of 2010.

Figure 12 illustrates the endpoint trajectory of the barrier in the entrance of the lagoon. The barrier head has extended 379 m

Table 2. Parameters and tidal conditions of images

Imaging time	Sensors	Resolution/m	Tide time (UTC+8)	Tide height/cm
1996-06-13	SPOT3 (HRV)	10	9:40	298
1996-06-27	SPOT3 (HRV)	10	9:40	519
2000-12-07	Landsat7 (ETM+)	15	10:17	343
2000-12-23	Landsat7 (ETM+)	15	10:17	508
2004-08-03	TERRA (ASTER)	15	10:50	571
2004-11-07	TERRA (ASTER)	15	11:50	263
2006-03-11	Landsat7 (ETM+)	15	10:16	509
2006-12-26	SPOT5 (HRG)	5	10:44	264
2008-03-06	1. Aerial orthophoto2.DEM	0.8/2.0	–	–
2010–01–14	WorldView–2	0.46	10:37	597
2010–12–02	ALOS(PRISM)	2.5	10:30	411
2013–03–07	Landsat7 (ETM+)	15	10:17	343
2013–12–03	SPOT6 (NAOMI)	1.5	10:28	635

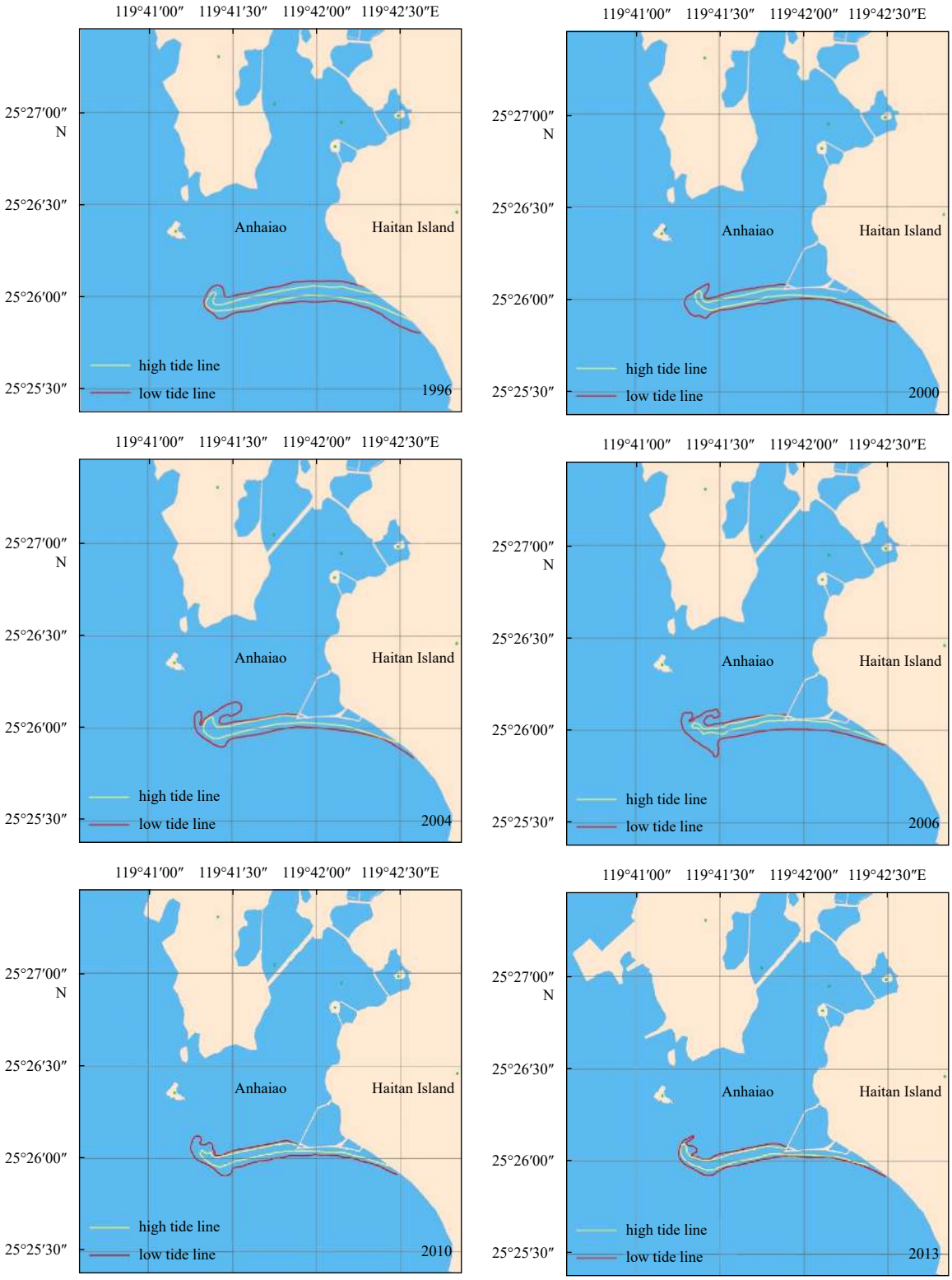

Fig. 9. Refine coastlines extracted from the images.

to the northwest strait since 1996. The deposition continued to occur on the north side because the reclamation in the north changed the longshore currents and resulted in the narrowing of the lagoon entrance, which disturbed the balance of the surrounding hydrodynamic environment.

3.3 *The deposition and erosion characteristics of the barrier*

After the analysis of the location and shape changes of the barrier, the deposition and erosion characteristics were determined and are described as follows. Figure 13 illustrates the intertidal terrain.

The results showed similar evolution trends analyzed from

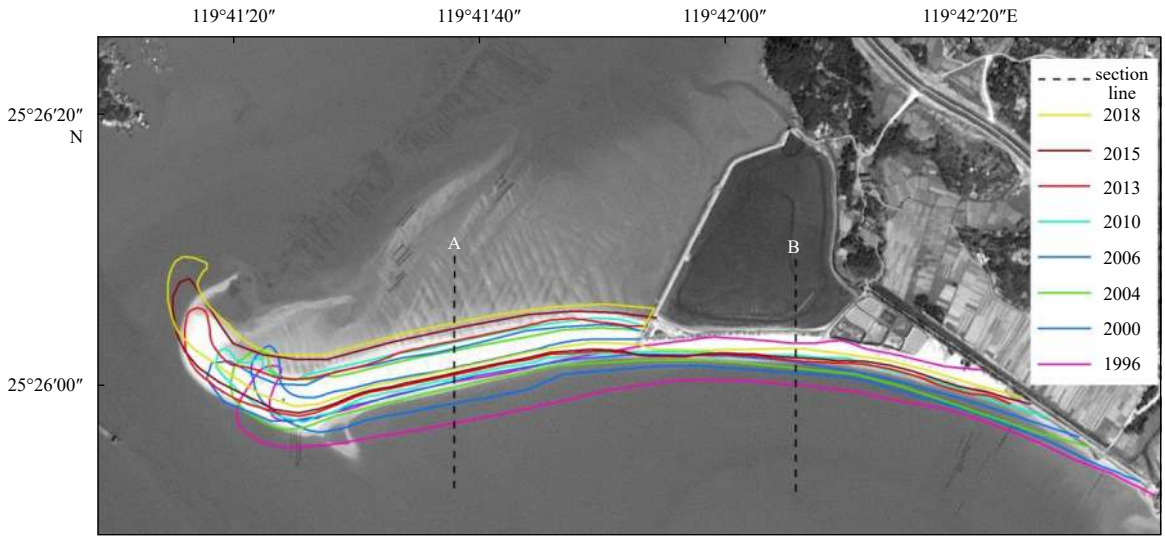

Fig. 10. Two selected profiles.

Table 3. Changes of the barrier

Year	Profile A		Profile B	
	Distance/m	Rate/m·a^{-1}	Distance/m	Rate/m·a^{-1}
1996	0.00	0.00	0.00	0.00
2000	38.28	9.57	26.88	6.72
2004	76.64	9.59	37.42	2.63
2006	94.74	9.05	45.97	4.28
2010	98.35	0.90	54.30	2.08
2013	99.69	0.45	58.34	1.35
2015	101.19	0.50	62.15	1.27
2018	102.60	0.47	65.45	1.10

the location and shape changes of the barrier. The intertidal zone of the main barrier body did not change as much as the barrier head. The inner part facing the lagoon area was deposited during the whole period, and erosion occurred in the outside part facing the open sea.

The deposition and erosion development of the barrier is shown in Fig. 14. The red outer region shows the erosion of the barrier, the inner blue region shows the deposition facing the lagoon area, while the gray of the barrier is the main body. The figure also shows similar geomorphological changes, i.e., northward movement with the head extending to the northwest open sea.

Figure 14a shows that the inner part of the barrier head and the south part of the main barrier body underwent erosion from 1996 to 2000, and the average erosion rate was approximately 41 358.8 m^3/a. The northern part was inside the lagoon, and the deposition in this region became high because of the large-scale human reclamation of mariculture dams in the northern lagoon. These human activities changed the hydrodynamic situation and lowered the lagoon tidal volume. The average deposition rate reached a maximum value of 69 334.4 m^3/a in this period.

Figure 14b shows the deposition and erosion situation of the barrier from 2000 to 2004. A man-made mariculture pool was developed in the end part of the barrier region in May 2004, which changed the longshore currents. Erosion occurred in the south and outside of the barrier head, and deposition occurred in the north. The shape of the barrier head changed as the deposition increased.

Figure 14c shows that erosion was maintained in the south part of the barrier, while deposition occurred in the north between 2004 and 2006, and the average erosion rate reached a

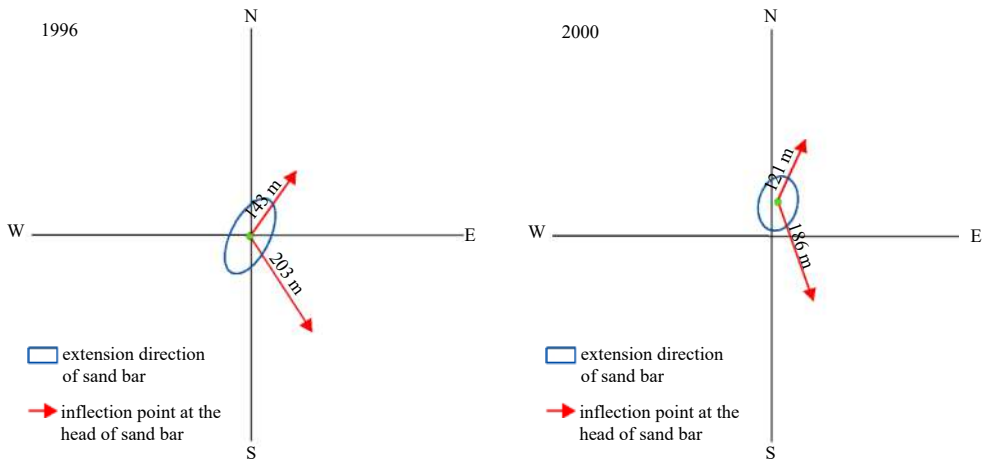

Fig. 11.

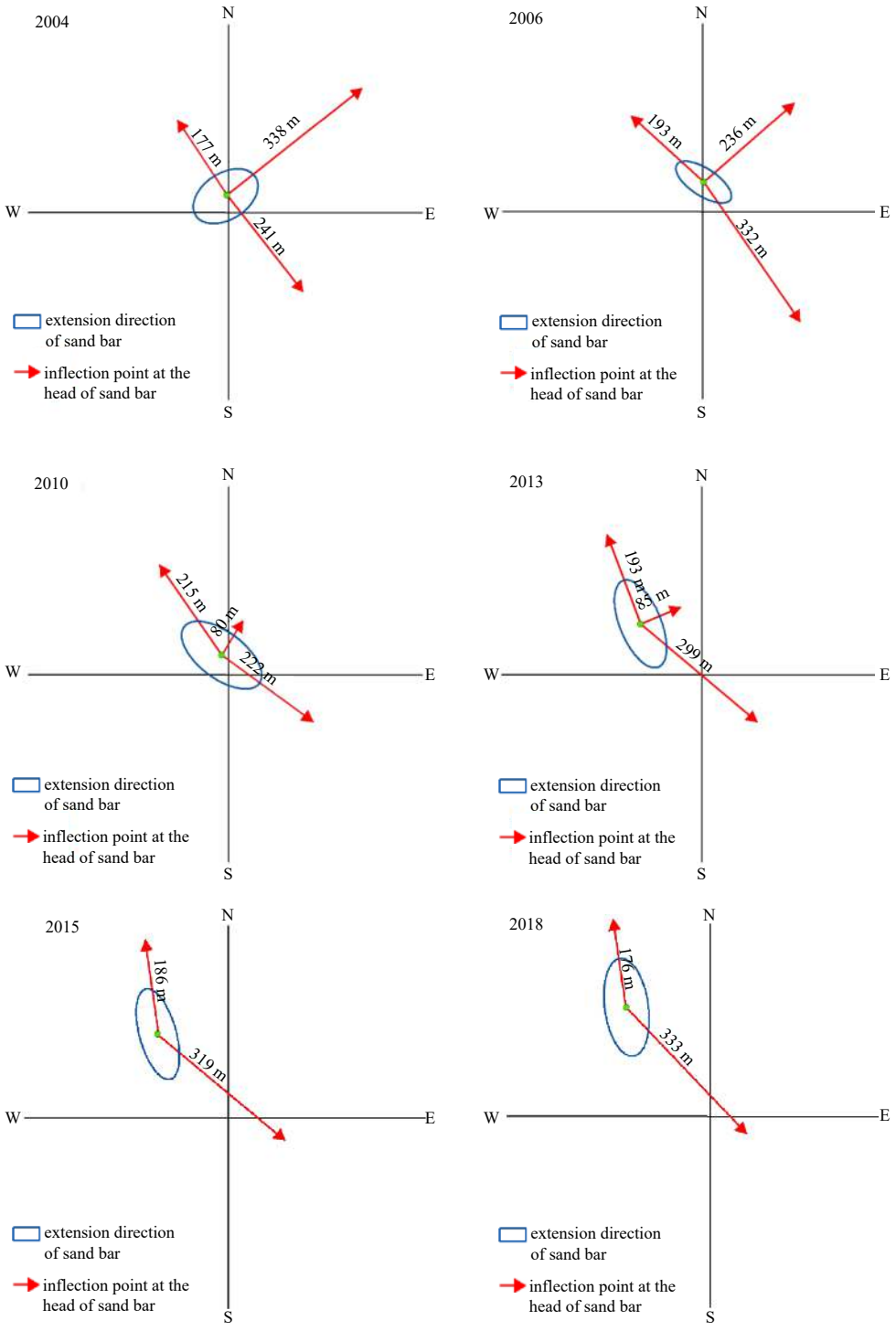

Fig. 11. Extension and inflection points of the barrier head.

higher level of 75 523.67 m^3/a. During this period, a new dam was constructed in the north of the lagoon.

Figure 14d and Figure 14e show similar evolution trends from 2006 to 2010 and from 2010 to 2013, respectively. Erosion still occurred in the south barrier and the inner side of the barrier head. The average erosion rate in this period was lower than that in the period from 2004 to 2006. With the decrease in human exploitation, the lagoon-barrier landscape and the hydrodynamic environment became increasingly stable, which resulted in less deposition in the northern part of the barrier facing the lagoon. The deposition mainly occurred around the barrier head. The average deposition rate from 2010 to 2013 was slightly higher than that from 2006 to 2010 because of the small-scale reclamation for the construction of Jinjing Port in the north (Table 4).

3.4 *Driving forces of the barrier morphological changes*

The development and evolution of the sand barrier-lagoon system is mainly dominated by natural factors (such as wave, tide, current) and human factors (such as land reclamation, unreasonable coastal engineering construction, sand mining), and

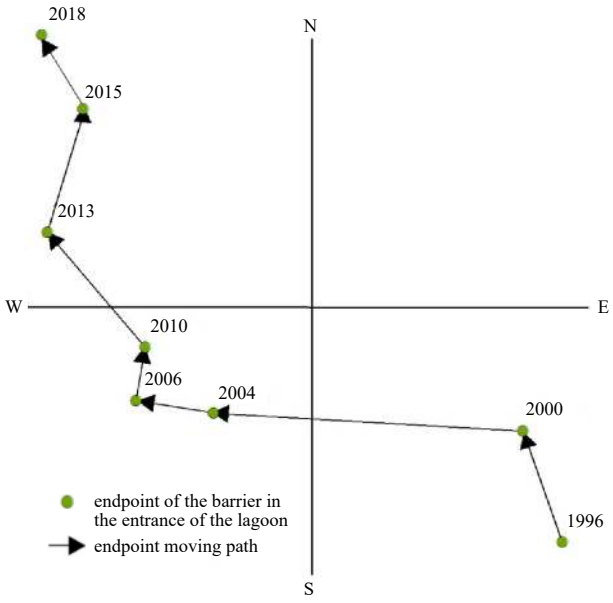

Fig. 12. Endpoint trajectory of the barrier in the entrance of the lagoon.

the latter have been accelerating the process of sand barrier-lagoon landform evolution.

Besides the reclamation projects, sediment source reducing caused by hard engineering along the upstream coast and sand mining offshore is another main driving force that caused sand barrier system landscape evolution. (1) Coastal engineering construction: generally, the sandy barrier was located in the sediment transport chain towards northwest along the south side of Pingtan Island. However, the seawall, shipyard and its affiliated groyne constructed on the upstream beach directly split the intact beach and blocked sand sediment transporting from southeast to northwest. (2) Sand mining: the rapid urban development of Pingtan had resulted in an increasing demand for sea sand. Unfortunately, the unregulated sand mining nearshore of Anhaiao occurred due to lack of management participation, which directly disturbed the nearshore sediment supply equilibrium, accelerating the sand barrier erosion.

Further quantitative analysis shows the impact of human activities on the Anhaiao sand barrier-lagoon system is mainly reflected in shortening of the lagoon coastline, decrease in the lagoon, and narrowing of the tidal inlet.

(1) Shortening of the lagoon coastline

From 1982 to 2018, the lagoon coastline had changed greatly caused by large-scale reclamation aquaculture activities in the Anhaiao Lagoon. In 1982, a seawall was built between the Jidiao Island and Haitan Island. The waterway on the north side of the lagoon was blocked, and Anhaiao became a semi-closed bay. From 1996 to 2004, the length of lagoon coastline had reduced from 12 880 m to 9 332 m with the length reduction rate of 27.55%, and the natural coastline retention rate had decreased from 88.68% to 78.66% (Fig. 15). Although there was no reclamation activity carried out in the lagoon after 2004, sand barrier had been moving westward for the period between 2004 and 2018, which brought about the increase of lagoon coastline length by 255 m.

(2) Decrease in the lagoon area

Since the 1980s, the large-scale aquaculture activities on the tidal flats of Anhaiao Lagoon resulted in decrease in the lagoon

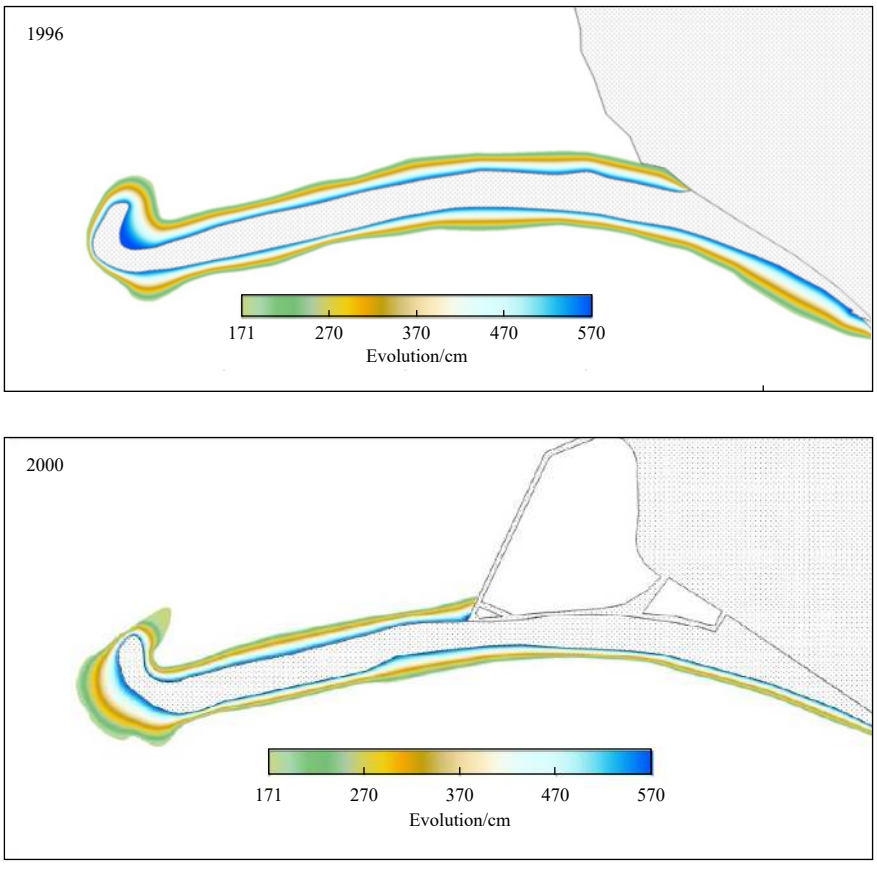

Fig. 13.

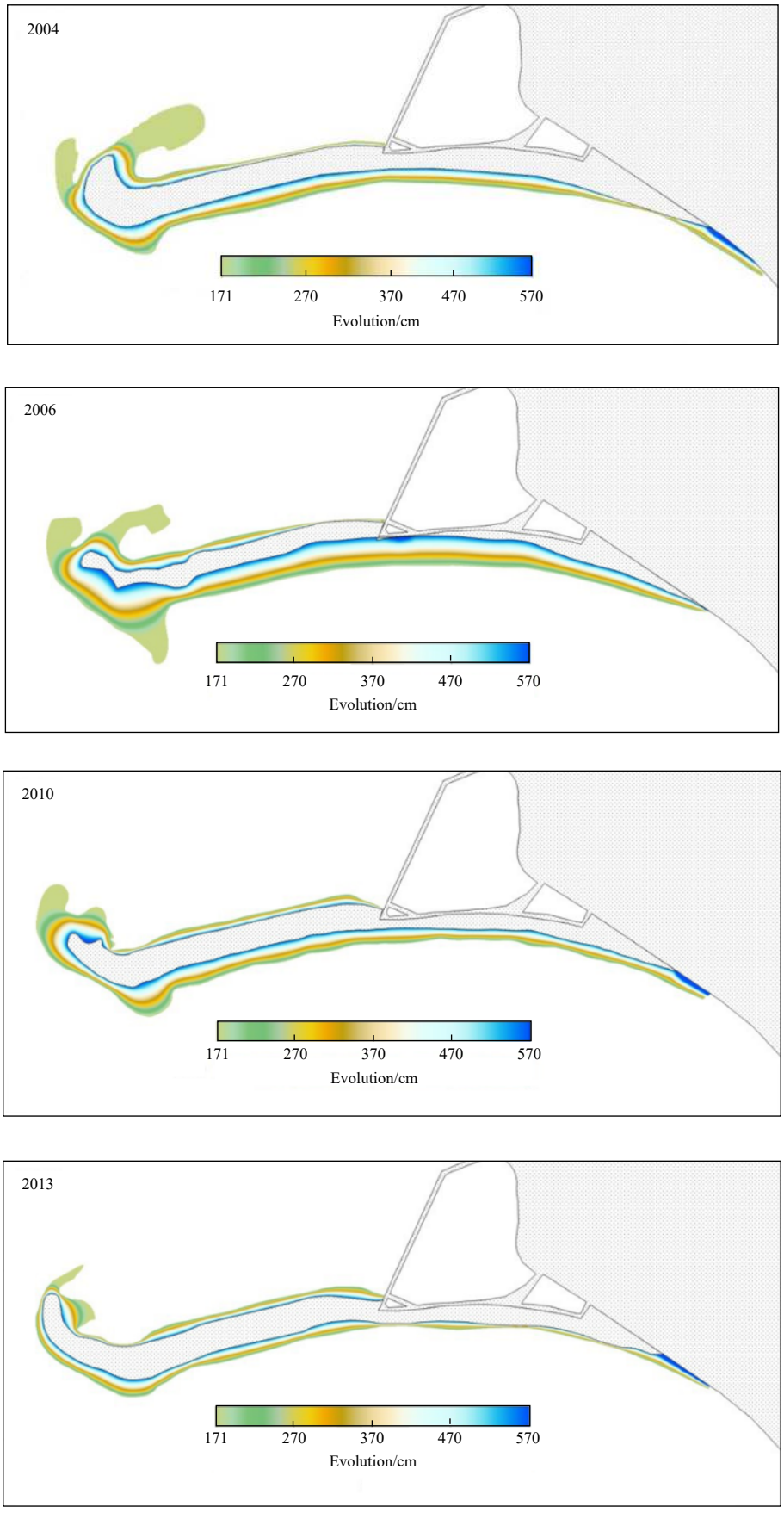

Fig. 13. Intertidal terrain of the barrier in different periods.

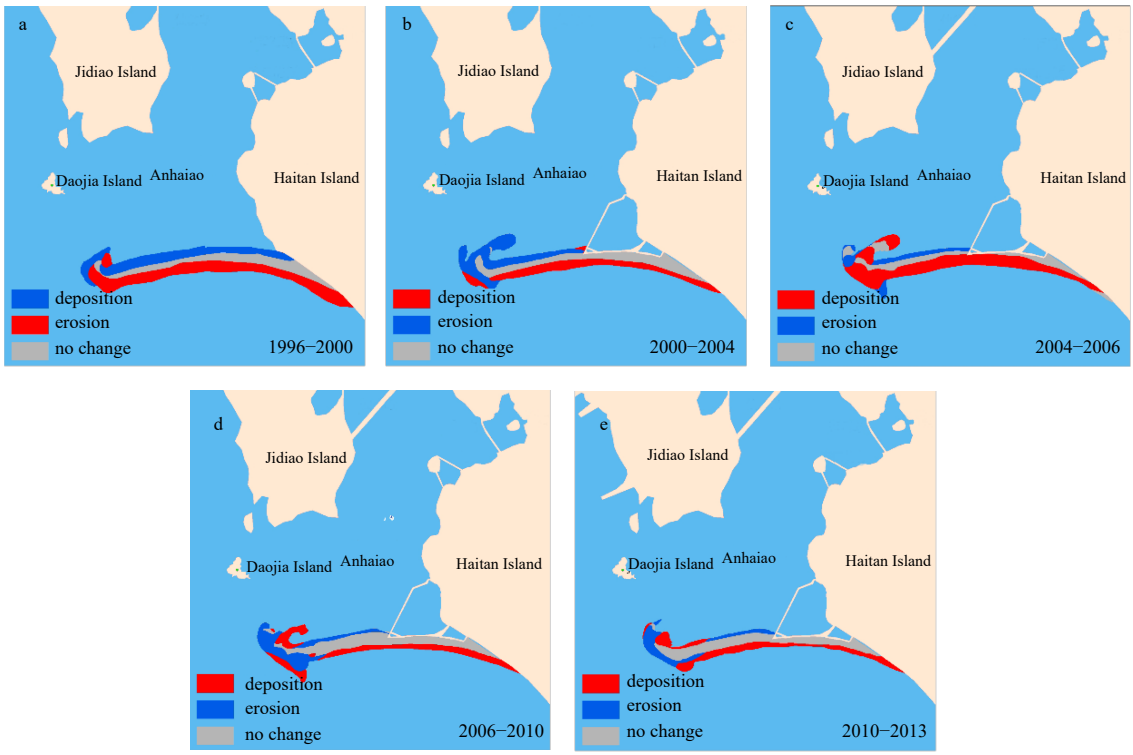

Fig. 14. Deposition and erosion of the barrier.

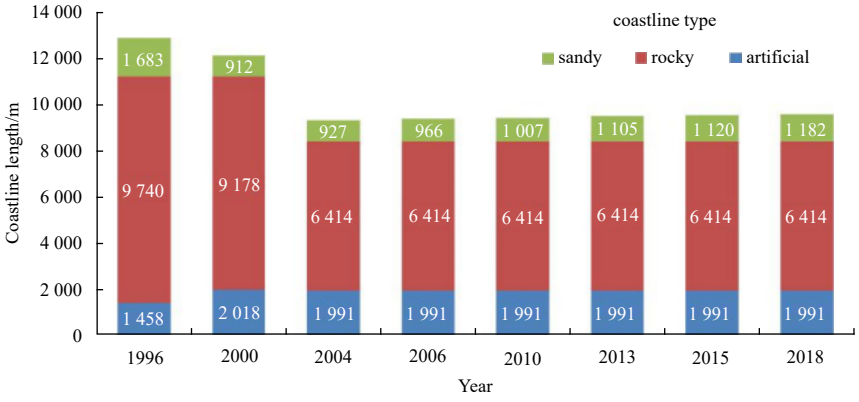

Fig. 15. Coastline changes of the lagoon between 1996 and 2018.

Table 4. Time series characteristics of the barrier erosion and deposition

Period	Erosion		Deposition	
	Volume/m^3	Average rate/$m^3 \cdot a^{-1}$	Volume/m^3	Average rate/$m^3 \cdot a^{-1}$
1996–2000	206 794	41 358.8	346 672	69 334.4
2000–2004	123 958	24 791.6	105 684	21 136.8
2004–2006	226 571	75 523.67	57 362	19 120.67
2006–2010	56 532	11 306.4	66 207	13 241.4
2010–2013	91 763	22 940.75	53 669	17 889.67

area from 2.81 km^2 to 2.60 km^2 during the period between 1996 and 2004 with a reduction rate of 25.27%. Since the aquaculture activities ended in 2004, with the stabilization of the sand barrier movement, there has been no significant change in the lagoon area which basically remained at 2.10 km^2.

(3) Narrowing of the tidal inlet

In 1982, a seawall was built between Jidiao Island and Haitan Island, the waterway on the north side was blocked, and Anhaiao became a semi-enclosed bay. In 1986, there were large-scale reclamation projects on the east side of Jidiao Island and the west side of Haitan Island. On the other hand, the erosion and deposition of the tidal inlet were affected by the aquaculture reclamation in the lagoon which reduced the tidal volume of the lagoon and changed the flow direction in the lagoon. Meanwhile, due to

the northwestward movement of the sand barrier, from 1996 to 2018, the barrier head continued to extend in the direction of Jidiao Island, and the width of tidal inlet decreased from 945 m to 657 m with a reduction of 30.5%.

3.5 *Management countermeasures*

In order to improve and enhance the ecological service function of sand barrier-lagoon in Anhaiao, several management countermeasures are proposed as follows:

(1) Coastal zone spatial planning

Firstly, it is suggested that new marine zoning of Anhaiao should be redesignated as "tourist recreation developing area" from "industrial and urban developing area" that could provide management and policy foundation for barrier-lagoon system protection and sustainable development. Secondly, based on the adjustment of the marine function zoning, the barrier-lagoon system, the adjacent waters and beaches should be taken as a whole ecological protection area.

(2) Environment remediation and restoration projects

In view of the environmental pressures faced by Anhaiao, the implementation of specific engineering projects listed in Table 5 are proposed, whose aim is to maintain the stability of the Anhaiao sand barrier-lagoon system and achieve the sustainable development goals of coastal resources.

Table 5. List of Anhaiao sand barrier-lagoon remediation and restoration projects

No.	Objectives	Countermeasures
1	Restore hydrodynamic equilibrium	(1) remove the mariculture facilities and embankments in the lagoon (2) lagoon dredging
2	Restore the sand barrier and maintain the sediment supply equilibrium	(3) remove the seawall built on the sand barrier (4) remove the shipyard on the upstream beach
3	Realize real-time dynamic monitoring and forcast system of sandy barrier-lagoon	(5) establish the monitoring system in the Anhaiao Bay

4 Conclusions

A refined coastline extraction method based on satellite images and ground survey data concerning tidal correction was used in this study, and six of coastlines were selected to analyze the changes in the barrier location. A more specific standard deviation ellipse algorithm was used to illustrate the evolution of the barrier head. Moreover, the erosion and deposition characteristics of the whole barrier were studied.

The results showed that the sand barrier retreated to the northward direction with the head extending to the northwest open sea. The lower movement in the end of the barrier was mainly caused by mariculture reclamation construction, where the stable and artificial bank decreased the integrality, stability and uniqueness of the sand barrier. After the reclamation in 2004, the movement rate of the barrier first started to increase and then decreased, reaching a peak in 2006 and finally stabilizing in 2010. The reclamation for the construction of Jinjing Port aggravated the deposition around the barrier head and the inner part of the lagoon, while erosion was maintained in the south of the barrier due to the changes in longshore currents caused by human constructions. During the period of 1996 to 2018, the middle of the barrier moved 102.60 m away from its original location, and the end of the barrier moved 65.45 m. Similar to the location changes, the head of the sand barrier moved 379 m to the northwest.

Limited by the coarse resolution of different images and the lack of ground survey data, further efforts should be made to conduct a detailed evolution analysis of the barrier and support decision making for the protection of the lagoon-barrier coastal area in the future.

According to results analysis of Anhaiao sand barrier morphological evolution, its driving forces were concluded with the purpose of maintaining the integrity of Anhaiao sand barrier-lagoon system, the management countermeasures are proposed from the aspects of spatial planning and environment restoration.

References

Ahmed M H, El Leithy B, Thompson J R, et al. 2009. Application of remote sensing to site characterisation and environmental change analysis of North African coastal lagoons. Hydrobiologia, 622(1): 147–171, doi: 10.1007/s10750-008-9682-8

Allen G H, Pavelsky T M. 2018. Global extent of rivers and streams. Science, 361(6402): 585–588, doi: 10.1126/science.aat0636

Alonso-Pérez F, Ruiz-Luna A, Turner J, et al. 2003. Land cover changes and impact of shrimp aquaculture on the landscape in the Ceuta coastal lagoon system, Sinaloa, Mexico. Ocean & Coastal Management, 46(6–7): 583–600

Brivio P A, Zilioli E. 1996. Assessing wetland changes in the Venice lagoon by means of satellite remote sensing data. Journal of Coastal Conservation, 2(1): 23–32, doi: 10.1007/BF02743034

Carrasco A R, Ferreira Ó, Roelvink D. 2016. Coastal lagoons and rising sea level: A review. Earth-Science Reviews, 154: 356–368, doi: 10.1016/j.earscirev.2015.11.007

Chang Yi, Chu Kawai, Chuang L Z H. 2018. Sustainable coastal zone planning based on historical coastline changes: A model from case study in Tainan, Taiwan. Landscape and Urban Planning, 174: 24–32, doi: 10.1016/j.landurbplan.2018.02.012

Chen Hao. 2011. Research on the changes of barrier-lagoon coast in recent years in Shuidong Bay, Yuexi (in Chinese) [dissertation]. Shanghai: East China Normal University

Chen V, Mueller V. 2018. Coastal climate change, soil salinity and human migration in Bangladesh. Nature Climate Change, 8(11): 981–985, doi: 10.1038/s41558-018-0313-8

Dai Zhijun, Chen Jinhui, Ren Jie. 2007. Analysis of the stable states in the nearshore sea-floor of bar-lagoon coast in Bohe, Yuexi. Journal of Oceanography in Taiwan Strait (in Chinese), 26(1): 1–6

Dronova I, Gong P, Wang L. 2011. Object-based analysis and change detection of major wetland cover types and their classification uncertainty during the low water period at Poyang Lake, China. Remote Sensing of Environment, 115(12): 3220–3236, doi: 10.1016/j.rse.2011.07.006

Duck R W, da Silva J F. 2012. Coastal lagoons and their evolution: A hydromorphological perspective. Estuarine, Coastal and Shelf Science, 110: 2–14, doi: 10.1016/j.ecss.2012.03.007

El-Asmar H M, Hereher M E. 2011. Change detection of the coastal zone east of the Nile Delta using remote sensing. Environmental Earth Sciences, 62(4): 769–777, doi: 10.1007/s12665-010-0564-9

El-Asmar H M, Hereher M E, El Kafrawy S B. 2013. Surface area change detection of the Burullus Lagoon, North of the Nile Delta, Egypt, using water indices: A remote sensing approach. The Egyptian Journal of Remote Sensing and Space Science, 16(1): 119–123, doi: 10.1016/j.ejrs.2013.04.004

FitzGerald D M, Buynevich I, Argow B. 2006. Model of tidal inlet and barrier island dynamics in a regime of accelerated sea level rise.

Journal of Coastal Research, 2: 789–795

Frihy O E, Dewidar K M, Nasr S M, et al. 1998. Change detection of the northeastern Nile Delta of Egypt: shoreline changes, Spit evolution, margin changes of Manzala lagoon and its islands. International Journal of Remote Sensing, 19(10): 1901–1912, doi: 10.1080/014311698215054

Ghezzo M, Guerzoni S, Cucco A, et al. 2010. Changes in Venice lagoon dynamics due to construction of mobile barriers. Coastal Engineering, 57(7): 694–708, doi: 10.1016/j.coastaleng.2010.02.009

Gu Dongqi, Zhao Xiaotao, Xia Dongxing, et al. 2005. The study on wetland landscape evolution of the Chaoyanggang Lagoon based on 3S technologies. Acta Oceanologica Sinica (in Chinese), 27(2): 91–97

Han Xingxing, Chen Xiaoling, Feng Lian. 2015. Four decades of winter wetland changes in Poyang Lake based on Landsat observations between 1973 and 2013. Remote Sensing of Environment, 156: 426–437, doi: 10.1016/j.rse.2014.10.003

Kent B J, Mast J N. 2005. Wetland change analysis of San Dieguito Lagoon, California, USA: 1928–1994. Wetlands, 25(3): 780, doi: 10.1672/0277-5212(2005)025[0780:WCAOSD]2.0.CO;2

Lefever D W. 1926. Measuring geographic concentration by means of the standard deviational ellipse. American Journal of Sociology, 32(1): 88–94, doi: 10.1086/214027

Lin Heshan, Xu Jinyan, Jiang Degang, et al. 2016. Sand dam dynamic monitoring in coastal areas based on time-series remote sensing images. In: 2016 IEEE International Geoscience and Remote Sensing Symposium (IGARSS). Beijing: IEEE

Murray N J, Phinn S R, DeWitt M, et al. 2019. The global distribution and trajectory of tidal flats. Nature, 565(7738): 222–225, doi: 10.1038/s41586-018-0805-8

Sibson R. 1981. A brief description of natural neighbor interpolation. In: Barnett V, ed. Interpreting Multivariate Data. New York: John Wiley & Sons

Storms J E A, Jan Weltje G, Terra G J, et al. 2008. Coastal dynamics under conditions of rapid sea-level rise: Late Pleistocene to Early Holocene evolution of barrier–lagoon systems on the northern Adriatic shelf (Italy). Quaternary Science Reviews, 27(11–12): 1107–1123

Sun Weifu. 2013. Monitoring and analyzing the lagoon dynamics in China using remote sensing imagery (in Chinese) [dissertation]. Shanghai: East China Normal University

Sun Weifu, Zhang Jie, Ma Yi, et al. 2016. Shoreline remote sensing extraction and accuracy verification method of coastal lagoon. Journal of Applied Oceanography (in Chinese), 35(3): 426–432

Tiner R W, Lang M W, Klemas V V. 2015. Remote Sensing of Wetlands: Applications and Advances. New York: CRC Press

Wang Y Q. 2009. Remote sensing of Coastal Environments. New York: CRC Press

Xu Hanqiu. 2005. A Study on information extraction of water body with the modified normalized difference water index (MNDWI). Journal of Remote Sensing (in Chinese), 9(5): 589–595

Zheng Duan, Bastiaanssen W G M. 2013. Estimating water volume variations in lakes and reservoirs from four operational satellite altimetry databases and satellite imagery data. Remote Sensing of Environment, 134: 403–416, doi: 10.1016/j.rse.2013.03.010